Available online at www.sciencedirect.com
ScienceDirect
Journal of the European Ceramic Society 27 (2007) 91–99
www.elsevier.com/locate/jeurceramsoc

Nickel aluminate spinel formation during sintering of simulated Ni-laden sludge and kaolinite

Kaimin Shih, James O. Leckie *

Department of Civil and Environmental Engineering, Stanford University, Stanford CA 94305-4020, United States

Received 4 February 2006; received in revised form 20 April 2006; accepted 29 April 2006
Available online 21 June 2006

Abstract

Incorporating Ni-laden waste sludge into kaolinite-based construction ceramic materials appears promising based on the identified nickel bearing phases, evaluated incorporation efficiency and nickel leachability of the products. Nickel aluminate spinel ($NiAl_2O_4$) results from sintering kaolinite and nickel oxide between 990 and 1480 °C, with more than 90% incorporation efficiency achieved at 1250 °C and 3 h sintering. At lower temperature (990 °C), $NiAl_2O_4$ formed from the reaction between nickel oxide and the defect spinel generated from the kaolinite–mullite reaction series. In addition to sintering temperature and time, four raw material mixing procedures were employed, and the ball-milled slurry samples had the highest nickel incorporation efficiency. Prolonged leach testing of NiO, $NiAl_2O_4$ and the product from sintered kaolinite + NiO mixtures was carried out using the TCLP extraction fluid #1 (pH 4.9) to evaluate the product stability, and the results revealed the superiority of spinel products over NiO in stabilizing nickel.

Keywords: $NiAl_2O_4$; Spinels; Al_2O_3; Sintering; X-ray methods; Waste materials

1. Introduction

A common control strategy to remove heavy metals from wastestreams is by precipitation processes that result in metal-laden sludges, considered to be hazardous wastes.[1,2] In 1988, it was estimated that 40% of the hazardous wastes generated in the United States consisted of heavy metal wastes.[3] At present, the majority of heavy metal wastes are disposed of in strictly controlled landfills. Besides the potential for contamination of surface water and groundwater via percolation through the disposed materials,[4] the high cost of land disposal of hazardous waste has encouraged many industries to seek alternative practices for their wastestream management.[5]

Sludges from physico-chemical treatment of wastewaters generated by electroplating operations are known to be highly toxic.[1,6] Among those hazardous heavy metals, nickel is one of the major metals generated from these electroplating operations. Nickel may reasonably be anticipated to be a carcinogen, and the ingestion of large amounts of nickel will affect the function of the lung, stomach, blood, liver, kidneys, immune system, and reproduction ability.[7]

Electroless nickel plating plays an increasingly important role in manufacturing, especially for the fabrication of corrosion resistant articles. Wastewaters generated by this type of operation can contain nickel concentrations of several thousand ppm or higher.[8,9] In 1992, it was estimated that the electroless nickel plating industry produced more than 20,000 t/year of waste in the U.S. alone with a growth rate of 5%/year.[9,10] The rapid increase of this type of waste is of worldwide concern and is receiving considerable attention. Ocean discharge of electroless nickel plating waste is prohibited under the London Dumping Convention, and regulations pertaining to such chemicals and wastes are becoming increasingly stringent.[11] The more than 10,000 electroplating shops in the United States,[12] are typically neither financially able nor technologically equipped to recycle or treat this type of discharge.[13]

Based on mineral phase changes during thermal treatment, many studies have successfully demonstrated the stabilization of radioactive waste in glass and ceramic materials for storing in geologic repositories.[14,15] In terms of recycling the waste and reducing waste volume, the development of sintering non-hazardous wastes into construction ceramics is also

* Corresponding author. Tel.: +1 650 723 2524; fax: +1 650 725 3164.
E-mail address: leckie@stanford.edu (J.O. Leckie).

0955-2219/$ – see front matter © 2006 Elsevier Ltd. All rights reserved.
doi:10.1016/j.jeurceramsoc.2006.04.176

quite successful.[16,17] Recently, investigators started to stabilize/solidify the heavy metals within thermally treated glass, clays or metal oxides, and undertook leachability tests on their heavy metal containing products.[18,19] However, the preparation of these stabilized materials are currently based on empirical approaches with the experiments of incorporating low-concentrations of heavy metals into multi-phase natural clays. The sintering systems with low-metal concentration, multiple metals, and complex mineral phases had unavoidably led to difficulty of identifying the incorporation mechanisms, although the products usually achieved the low leachability and desired mechanical properties.[18] In addition, leachability of the metal-accommodating mineral phases in these previous products were not thoroughly investigated. Furthermore, many of the mineral phases were not clearly identified. As a promising and economically feasible strategy of incorporating heavy metals into construction ceramic materials, this approach requires more extensive investigation and development in understanding the scientific basis.

Most common ceramic construction products are made from natural clays and silicates. Kaolin, consisting chiefly of kaolinite ($Al_2Si_2O_5(OH)_4$), is a common clay type, and the raw materials of most ceramics include high percentages of kaolinite (40–65%).[20,21] Production of ceramics involves a process of timed heating procedures (sintering). During the sintering process, physically bound water is removed at 110 °C, followed by decomposition of kaolinite with the loss of chemically bound water and transformation to amorphous metakaolin above 550 °C.[22,23] Beyond 980 °C, the metakaolin is converted to a poorly crystalline defect spinel phase.[24,25] At 1000 °C, mullite starts to form; around 1150–1300 °C (depending on the impurity level), amorphous silica crystallized as cristobalite.[26] During the treatment of metal bearing wastewater, lime is often added to precipitate metals, and thus the dominant forms of nickel in sludge are usually the hydroxide and carbonate forms.[1] Researches have simulated nickel-laden sludge by using lime to precipitate nickel from its nitrate and chloride solutions,[2,6] or by directly using nickel hydroxide.[27] When thermally treated, these sludges decompose directly to nickel oxide (NiO). NiO is the most inert phase among the common nickel waste compounds, and remains stable until melting at around 1960 °C.[28]

The goal of this study was to develop a fundamental understanding of the association between NiO and kaolinite during the ceramic sintering process. The approach was to simulate the stabilization of Ni-laden sludge by sintering with kaolinite-base clays, and to identify how nickel was incorporated in the sintered products. The raw materials with high nickel concentration were sintered between 900 and 1480 °C to investigate nickel incorporation efficiency. The high temperature (1480 °C) sintered products were leached by a 25-day leaching test modified from U.S. EPA SW-846 Method 1311, toxicity characteristic leaching procedure (TCLP).[29] Insights gained from this study will lead to the ability to optimize the production process of nickel containing ceramics, and to facilitate the incorporation reaction(s). The effects of raw material composition, mixing procedure, sintering temperature regime, and leaching test procedure are discussed.

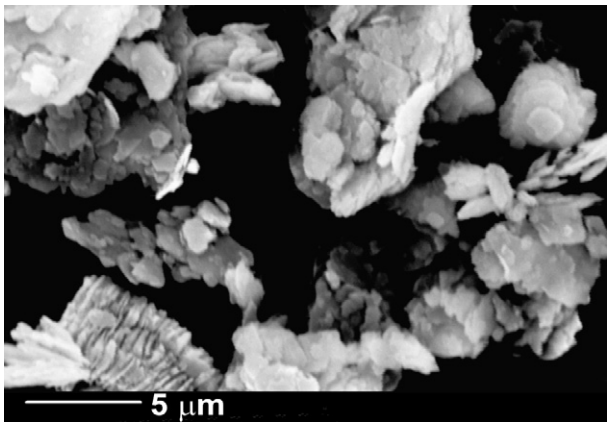

Fig. 1. Secondary electron image of acid washed kaolin powder showing the typical fine-grained platy-like particles of kaolinite with strong aggregation. Individual particle size is usually around 1–2 μm or smaller, and the aggregate size can be from several micrometers to tens of micrometers.

2. Experimental methods

Nickel oxide (NiO) was used to simulate nickel-laden sludge. Experiments were carried out by firing the mixtures of nickel oxide with kaolinite, or γ-alumina (γ-Al_2O_3). NiO powder (Fisher Scientific) gave a measured surface area of $3.6 \pm 0.5\ m^2/g$ after 300 °C heating and He-gas purging for 3 h degassing. The surface area was measured by a Beckman Coulter SA3100™ Surface Area and Pore Size Analyzer using the BET method. USP grade acid washed kaolinite powder from Fisher Scientific yielded a BET surface area of $9.0 \pm 2.9\ m^2/g$. The larger measurement error and relatively low BET surface area of kaolin can be attributed to the aggregation of fine kaolinite platelets (Fig. 1). The chemical composition for kaolinite (Table 1) was determined from a solution prepared by Microwave-Assisted Acid Digestion (U.S. EPA Method 3052) in which 0.5 g of kaolin powder preheated at 700 °C for 12 h was mixed with 40 mL aqua regia and 10 mL hydrofluoric acid in a Teflon vessel and microwaved to total digestion. The digestion solution was diluted to 500 mL with MilliQ® water prior to analysis by a TJA IRIS Advantage/1000 Radial ICP Spectrometer. In order to compare the nickel incorporation mechanisms between kaolinite and alumina precursors, γ-Al_2O_3 was prepared from

Table 1
Chemical composition (wt.%) of USP grade acid washed kaolin powder

SiO_2	45.1
Al_2O_3	38.7
Fe_2O_3	0.60
TiO_2	0.58
SnO_2	0.52
Na_2O	0.41
CaO	0.11
K_2O	0.08
MgO	0.02
CoO	0.02
Cr_2O_3	0.01
ZnO	0.01
NiO	0.01

Loss on ignition: 13.8%.

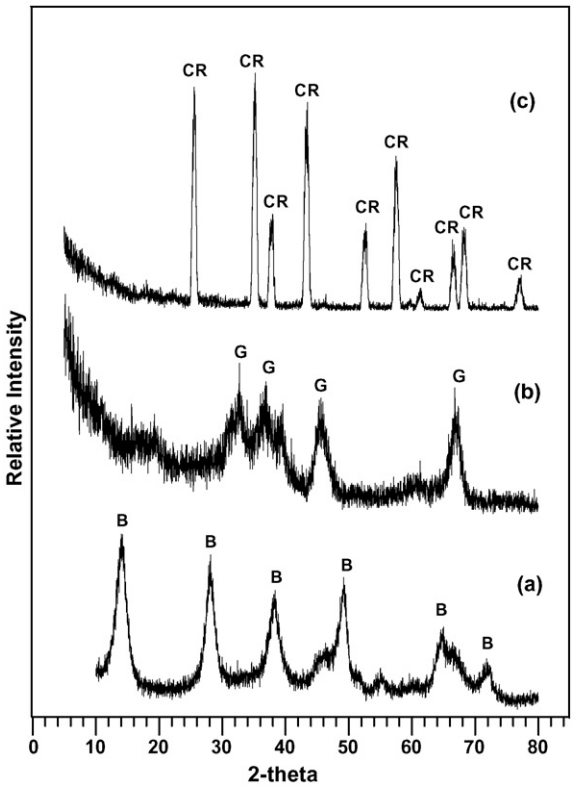

Fig. 2. The XRD pattern of (a) HiQ®-7223 alumina powder; (b) HiQ®-7223 alumina powder heated at 975 °C for 3 h; and (c) heated at 1480 °C for 6 h. "B" represents boehmite (ICDD PDF#74-1895); "G" for γ-alumina (γ-Al_2O_3); "CR" for corundum (α-Al_2O_3; ICDD PDF#83-2080).

HiQ®-7223 alumina powder (Alcoa Corporation), which has a reported surface area of 228 m^2/g and d_{50} particle diameter of 54.8 μm. As received HiQ®-7223 alumina was confirmed by XRD to be boehmite (AlOOH; ICDD PDF#74-1895), Fig. 2(a), which after heat treatment at 975 °C for 3 h was successfully converted to a γ-Al_2O_3 dominant material.[30,31] Further calcination above 1200 °C observed corundum (α-Al_2O_3; ICDD PDF#83-2080) peaks (Fig. 2(c)).

The precursors and NiO were normally mixed to a total dry weight of 200 g, together with 1 L of MilliQ® water and 25 zirconia milling balls (o.d. × *H*: 0.5 in. × 0.5 in.), in a 4 L porcelain milling jar. The milling jar was rotated in a speed of ~60 rpm for 22 h, and then the slurry samples were molded into 2 cm × 2 cm × 2 cm cubes and dried at 95 °C for 3 days. These cubes were either fired directly at 1480 °C/48 h prior to leach testing, or pressed into 13 mm pellets at 125 MPa for sintering efficiency investigation. After sintering, the samples were air-quenched and ground into powders for X-ray diffraction (XRD) analysis and leach testing. In practice, construction ceramics will likely incorporate quite low levels of metal, so that product properties are not compromised. However, in order to investigate the incorporation mechanism in nickel-rich phases, the raw materials in this study were prepared with a Ni/Al mole ratio of 1:2, this being the stoichiometric maximum for the $NiAl_2O_4$ spinel.

Phase transformations during sintering were monitored by XRD. The diffraction patterns were collected using a Rigaku Geigerfex diffractometer (Rigaku Denki Co. Ltd.) equipped with Cu X-ray tube operated at 35 kV and 15 mA. Scans were collected by a MDI XRD diffractometer control and data acquisition system (Material Data, Inc.) from 10° to 80° 2θ-angle, with the step size of 0.02° and a counting time of 1 s/step. Phase identification was executed by matching XRD patterns with the powder diffraction files (PDF) database of International Centre for Diffraction Data (ICDD). Diffraction patterns were processed using JADE (version 6.5.3) developed by Material Data, Inc. with a whole pattern fitting (WPF) function using the Pawley method, to determine the weight percent of each crystalline phase.[32] The weighted (*R*) and expected (*E*) reliability values were calculated using the following equations:

$$R\,(\%) = 100 \times \sqrt{\frac{\sum w(i) \times (I(\mathrm{o}, i) - I(\mathrm{c}, i))^2}{\sum w(i) \times (I(\mathrm{o}, i) - I(\mathrm{b}, i))^2}} \quad (1)$$

$$E\,(\%) = 100 \times \sqrt{\frac{N - P}{\sum I(\mathrm{o}, i)}} \quad (2)$$

where $I(\mathrm{o}, i)$ is the observed intensity of a fitted data point (i), $I(\mathrm{c}, i)$ the calculated intensity at this data point, $I(\mathrm{b}, i)$ the background intensity at this data point, $w(i)$ the weight of this data point as $w(i) = 1/I(\mathrm{o}, i)$, N the number of fitted data points, P the number of refined parameters, and $\sum I(\mathrm{o}, i)$ in E is the sum of over all fitted data points (N) that are 2σ above the fitted background. The R/E ratio or "goodness of fit" will equal one in an ideal refinement, although, practically, background and the peak profile mismatch lead to $R/E > 1$.

In order to evaluate the long-term stability, the $NiAl_2O_4$ containing products were leached by a 25-day leaching test modified from U.S. EPA SW-846 Method 1311, toxicity characteristic leaching procedure (TCLP) with a pH 4.9 acetic acid solution (extraction fluid #1) as the leaching fluid prepared from 5.7 mL glacial acetic acid with 64.3 mL of 1 N NaOH, and then diluting it with MilliQ® water to a volume of 1 L. In this procedure, the test samples were first crushed into coarse particles, and then dry ball-milled for 8 h to ensure the homogeneous reduction of particle size. Each leaching vial was filled with 10 mL TCLP extraction fluid and 0.5 g powder. The leaching vials were tumbled end-over-end at 60 rpm for agitation periods of 0.75–25 days. At the end of each agitation period, the leachates were filtered with 0.2 μm syringe filters, pH was measured, and the concentrations of Ni were derived from TJA IRIS Advantage/1000 Radial ICAP spectrometer with CLARITAS® certified reference solution (SPEX CertiPrep, Inc.).

3. Results and discussion

3.1. Thermal treatment of kaolinite

Kaolinite is a major raw material for commercial construction ceramics.[21] The phase transformation of kaolinite under thermal treatment has been extensively studied and the reaction sequence is known as the kaolinite – mullite reaction series.[22–25] However, the kaolinite – mullite reaction series is not completely understood, the most controversial point being the existence of a

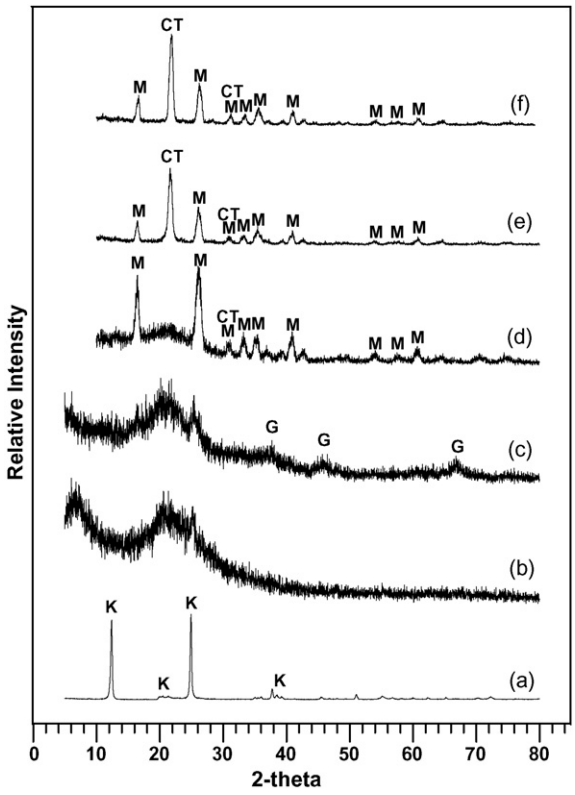

Fig. 3. X-ray diffraction (XRD) patterns of (a) USP grade acid washed kaolin powder, after being calcined at (b) 600 °C for 3 h, (c) 990 °C for 3 h, (d) 1000 °C for 3 h, (e) 1300 °C for 3 h, and (f) 1480 °C for 3 h. "K" represents peak position of referenced kaolinite (ICDD PDF#78-1996); "G" for γ-alumina (γ-Al_2O_3); "M" for mullite ($3Al_2O_3{\cdot}2SiO_2$; ICDD PDF#79-1455); "CT" for cristobalite (SiO_2; ICDD PDF#76-0938).

defect spinel phase beyond 980 °C.[24] The mineral phase change of kaolinite during thermal treatment up to 1480 °C was investigated by XRD shown in Fig. 3. The XRD pattern of the raw (initial) kaolin powder (pattern (a)) showed a good match with standard kaolinite peaks (ICDD PDF#78-1996). With the sintering at 600 °C for 3 h, the sample became amorphous as shown in the XRD pattern (b). This was consistent with the noncrystalline nature of metakaolin ($2Al_2O_3{\cdot}4SiO_2$), which is generally believed to be a dehydration product from kaolinite at sintering temperatures above 550 °C. Beyond 980 °C, the metakaolin is converted to a poorly crystallized phase with the literature suggesting that one of two reactions is operating:

$$\underset{\text{(metakaolin)}}{2Al_2O_3 \cdot 4SiO_2} \xrightarrow{980\,^\circ C} \underset{\text{(defect silicon spinel-type structure)}}{0.375Si_8[Al_{10.67}\square_{5.33}]O_{32}} + \underset{\text{(amorphous)}}{SiO_2} \quad (3)$$

$$\underset{\text{(metakaolin)}}{2Al_2O_3 \cdot 4SiO_2} \xrightarrow{980\,^\circ C} \underset{\text{(defect spinel-type structure)}}{0.188Al_8[Al_{13.33}\square_{2.66}]O_{32}} + \underset{\text{(amorphous)}}{4SiO_2} \quad (4)$$

where □ = vacancy and the defect spinel phase without silicon is identical to γ-Al_2O_3. The poorly crystalline nature of the solid results in the difficulty of distinguishing the two similar defect spinel phases by XRD analysis, due to the weak and broad XRD peaks as shown in pattern (c). The XRD pattern of kaolinite sintered at 990 °C for 3 h showed the weak but still observable peaks around $2\theta = 37°$, 46°, 67°, same as the locations of γ-Al_2O_3 signature peaks,[30,31] although we do not have the Si–Al spinel (defect silicon spinel-type structure) diffraction data to do further comparison. We do not intend to comment on the spinel phase controversy by this 990 °C sintered XRD pattern alone, but this result does at least reflect the same kaolinite–mullite reaction series in the thermal treatment of this kaolinite. At a sintering temperature of 1000 °C for 3 h, the mullite phase ($3Al_2O_3{\cdot}2SiO_2$; ICCD PDF#79-1455) started to form within amorphous silica as shown in pattern (d) in Fig. 3. When the temperature reached 1300 °C, the amorphous silica crystallized as cristobalite (SiO_2; ICDD PDF#76-0938) as shown in pattern (e), and this phase composition was maintained through the highest sintering temperature of 1480 °C in this study (pattern (f)).

3.2. $NiAl_2O_4$ spinel formation

XRD spectra for sintered kaolinite, and the mixture of kaolinite + NiO are shown in Fig. 4. The $NiAl_2O_4$ spinel (ICDD PDF#78-0552) was found in the product of the 990 °C and 6 h sintered kaolinite + NiO sample (Fig. 4(d)). The extended 6 h sintering time here was designed to further facilitate attainment of equilibrium in order to ascertain the stable phase(s) at that sintering temperature. At 900 °C, the amorphous metakaolin was

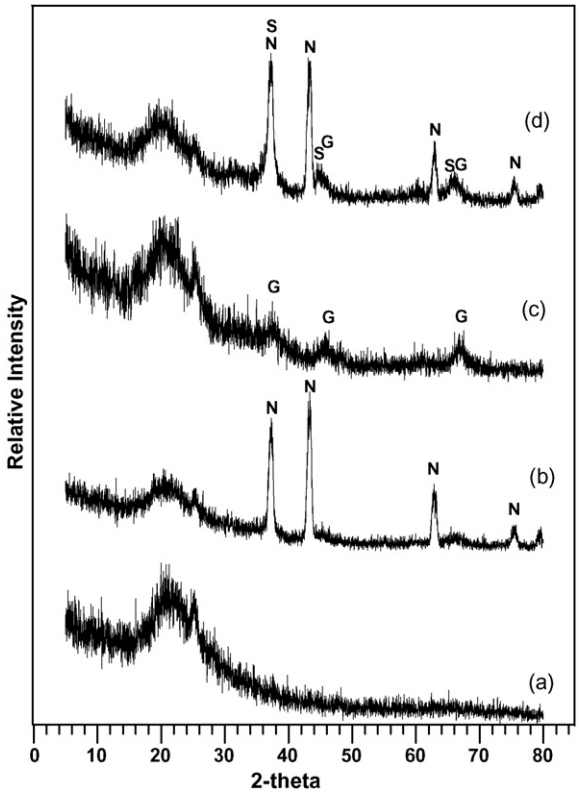

Fig. 4. XRD patterns of 6 h 900 °C sintered (a) kaolinite, (b) kaolinite + NiO, and 990 °C sintered (c) kaolinite, and (d) kaolinite + NiO. "N" represents NiO (ICDD PDF#78-0429); "G" for γ-alumina (γ-Al_2O_3); "S" for nickel aluminate spinel ($NiAl_2O_4$, ICDD PDF#78-0552).

detected as the only phase in the kaolinite–mullite reaction series (pattern (a)), and there was no $NiAl_2O_4$ spinel identified in the sintered kaolinite + NiO sample (pattern (b)). At 990 °C, while the γ-Al_2O_3 or the defect Si–Al spinel patterns showed (pattern (c)), the $NiAl_2O_4$ spinel was formed at the same time (pattern (d)). The strongest intensity peak ($2\theta = 37.01°$) of $NiAl_2O_4$ spinel was strongly overlaid by the NiO peak at $2\theta = 37.25°$, and probably also overlaid by the γ-Al_2O_3 peak at $2\theta \sim 37°$. However, the obvious increase in intensity at this peak region ($2\theta = 36.9–37.5°$) in pattern (d) provided the evidence of the $NiAl_2O_4$ spinel formation. In addition, although the $NiAl_2O_4$ spinel peak locations at $2\theta = 45.01°$ and 65.54° were also very close to γ-Al_2O_3 peaks ($2\theta \sim 46°$ and 67°), these two $NiAl_2O_4$ spinel peaks can still be identified from pattern (d) of Fig. 4.

Sintering of kaolinite + NiO at 990 °C revealed that $NiAl_2O_4$ spinel is the only phase incorporating nickel during the kaolinite–mullite reaction series (Fig. 4(d)), and also suggests two possible incorporating mechanisms at this sintering temperature:

$$NiO + \gamma\text{-}Al_2O_3 \rightarrow NiAl_2O_4 \quad (5)$$

$$5.33NiO + Si_8Al_{10.67}O_{32} \rightarrow 5.33NiAl_2O_4 + 8SiO_2 \quad (6)$$

$NiAl_2O_4$ formed by reactive sintering of nickel oxide and alumina (Al_2O_3) has been studied extensively. Phillips et al. compiled the early data and published the first phase diagram of NiO–Al_2O_3 system over the range of 1350–2100 °C,[28] which showed the possibility of spinel formation above 1350 °C. The $NiAl_2O_4$ phase has high resistance to acids and alkalis,[33] and most recent studies on $NiAl_2O_4$ properties were obtained from samples synthesized from sintering the coprecipitate of nickel nitrate and aluminum nitrate solutions, the so-called sol–gel method. [33,34] Aluminum oxide has several common forms including α-alumina (α-Al_2O_3, a hexagonal crystalline structure also known as corundum), seven transition Al_2O_3 phases (γ, δ, κ, ρ, η, θ, and χ), and several hydrated forms, such as aluminum trihydroxide (bayerite) and monohydroxide (boehmite).[30,31] To date, oxide sintering studies of $NiAl_2O_4$ have not emphasized the role of the different transition aluminas.[35,36]

In order to investigate the possibility of nickel incorporation by γ-Al_2O_3, as one of the hypothesized nickel incorporation mechanism (Eq. (5)) at 990 °C, we sintered a mixture of γ-Al_2O_3 and NiO at 990 °C for 6 h, and found the formation of $NiAl_2O_4$ spinel (Fig. 5). At 990 °C and 6 h sintering, the aluminum oxide still remains as the γ type with low diffraction intensity similar to the pattern (b) in Fig. 2. However, the sintered γ-Al_2O_3 + NiO sample in Fig. 5 showed clear XRD peaks of the $NiAl_2O_4$ spinel and the unreacted NiO. This result confirmed $NiAl_2O_4$ formation from the reaction between γ-Al_2O_3 and NiO suggested in Eq. (5) at 990 °C. It may also provide a possible explanation for the presence of $NiAl_2O_4$ during sintering of kaolinite and NiO mixtures at 990 °C, if γ-Al_2O_3 appeared in the kaolinite–mullite reaction series. However, due to the difficulty of obtaining the defect silicon spinel ($Si_8Al_{10.67}O_{32}$), the sintering of defect silicon spinel and NiO mixture was not conducted in this study.

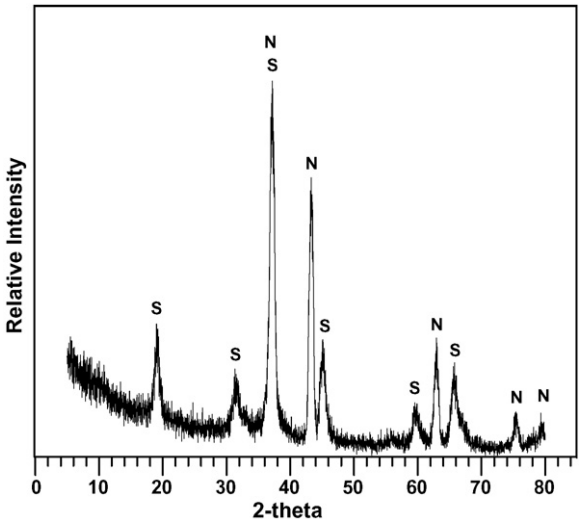

Fig. 5. XRD result of sintering the mixture of γ-Al_2O_3 and NiO at 990 °C for 6 h. "N" represents nickel oxide (ICDD PDF#78-0429); "S" for nickel aluminate spinel ($NiAl_2O_4$, ICDD PDF#78-0552).

3.3. Effects of mixing and sintering temperature

Since nickel oxide still showed strong XRD peaks at 990 °C sintering, we increased the sintering temperature to facilitate mass transfer mechanisms, like grain boundary diffusion and lattice diffusion.[37] During the use of precursors γ-Al_2O_3 and kaolinite at higher sintering temperatures, nickel oxide may be reacting with α-Al_2O_3 and mullite respectively as the main Ni incorporation mechanisms. Beside temperature effects, the compositional heterogeneity of the raw materials, determined by the extent of mixing, was also found to be critical for crystal growth in other ceramic studies.[38] In this study, we performed four raw material mixing procedures and sintered samples at temperatures ranging from 1200 to 1480 °C for 3 h. Subsequently, XRD phase quantification was performed by utilizing the WPF analysis of JADE to investigate the incorporation efficiency of nickel by the spinel phase. In addition to the ball-milled slurry samples (A and A1), the powder mixtures were also ball-milled for 22 h in dry powder form (B), lightly ground by mortar and pestle (C; around 200-circle grinding/10 g powder), or just mixed loose as dry powders with only slightly stirring (D). The γ-Al_2O_3 + NiO samples were prepared with all four mixing procedures (A–D); the kaolinite + NiO sample was prepared only with ball-milled slurry (A1), since mixing was expected to affect these two systems in the same way.

When NiO was transformed into $NiAl_2O_4$ by either γ-Al_2O_3 or kaolinite precursor, a transformation ratio (TR) index was used to indicate the nickel incorporation efficiency:

$$TR\,(\%) = \frac{\frac{\text{wt.\% of } NiAl_2O_4}{\text{MW of } NiAl_2O_4}}{\frac{\text{wt.\% of } NiAl_2O_4}{\text{MW of } NiAl_2O_4} + \frac{\text{wt.\% of NiO}}{\text{MW of NiO}}} \quad (7)$$

where MW is the molecular weight. A TR of 100% reflects complete incorporation of nickel as $NiAl_2O_4$; for TR of 0%, no nickel incorporation occurred. For the mortar and pestle ground γ-Al_2O_3 + NiO sample (C), the WPF results for 1200–1480 °C

Table 2
Whole pattern fitting (WPF) results of sintered γ-Al_2O_3 + NiO samples mixed by mortar and pestle grinding (sample C)

	Temperature (°C)						
	1200	1250	1300	1350	1400	1450	1480
NiO (wt.%)	14.4	11.3	9.1	7.7	5.7	5.3	4.3
α-Al_2O_3 (wt.%)	42.4	31.9	27.8	22.1	19.6	79.6	9.2
$NiAl_2O_4$ (wt.%)	43.2	56.8	63.1	70.2	74.7	15.1	86.5
TR (%)	56.0	68.1	74.6	79.4	84.7	86.4	89.5
R (%)	22.38	23.08	23.54	24.03	25.51	25.42	24.38
E (%)	14.44	13.69	13.84	13.28	14.05	13.74	12.71
R/*E*	1.55	1.69	1.70	1.81	1.82	1.85	1.92

The transformation ratio (TR) values were calculated by the estimated nickel oxide and spinel weight percentages to evaluate the incorporation efficiency. The weighted (*R*) and expected (*E*) values were also obtained to monitor the goodness of fit (*R*/*E*).

and 3 h sintered samples are listed in Table 2. The results clearly show TR increasing as sintering temperature increased, and the goodness of fit (*R*/*E*) staying within the 1.5–2.0 range. In the powder crystallography, the goodness of fit value between 2.9 and 1.0 is satisfactory.[39] The *R*/*E* values indicate that the WPF function is less accurate in estimating very high TR samples due to the relatively weaker diffracted intensities of NiO and α-Al_2O_3. However, WPF results were adequate for identifying the incorporation efficiency of nickel into the spinel phase with reasonable accuracy without precise estimation of phases in very small quantities.

Fig. 6 shows the TR values for samples A, B, C, D, and A1 sintered at 1200–1480 °C for 3 h, and it is clear that the mixing procedure strongly affected the incorporation efficiency

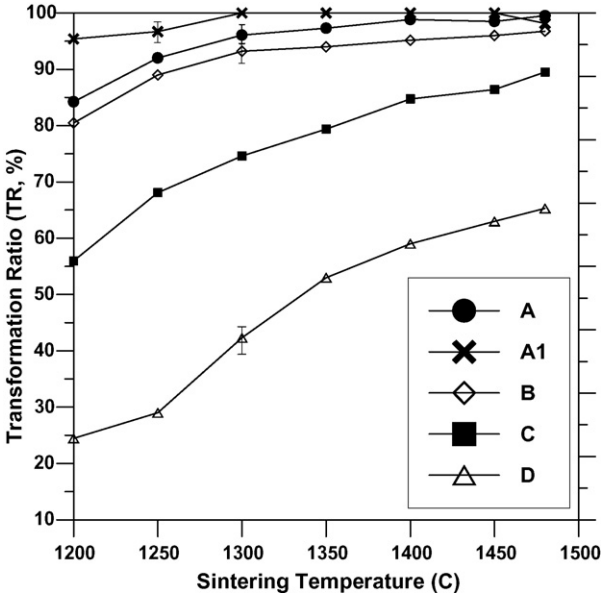

Fig. 6. Mixing and sintering temperature effects on nickel incorporation efficiency. Transformation ratio (TR) values were plotted for the 22 h ball-milled γ-Al_2O_3 + NiO slurry samples (A), the 22 h ball-milled γ-Al_2O_3 + NiO powder samples (B), the lightly mortar and pestle ground γ-Al_2O_3 + NiO powder samples (C; around 200-circle grinding/10 g powder), the slightly stirred γ-Al_2O_3 + NiO powder samples (D), and the 22 h ball-milled kaolinite + NiO slurry samples (A1) sintered at 1200–1480 °C for 3 h.

of nickel. The 22 h ball milled samples had high incorporation efficiency, especially for those mixed in slurry form. Both ball-milled γ-Al_2O_3 + NiO slurry (A) and kaolinite + NiO slurry (A1) samples had ≥90% nickel incorporated into $NiAl_2O_4$ spinel at sintering temperatures higher than 1250 °C. The slightly higher incorporation efficiency of sample A1 compared to sample A may reflect the role of silica glass as a flux during sintering.[21] The introduction of a flux in solid state sintering would facilitate the diffusion and enhance Ni incorporation. The results clearly show the slightly less effective mixing of ball-milling dry powders (B), and, to a much greater extent, the lightly ground powder sample (C) and slightly stirred powder sample (D). At sintering temperatures below 1200 °C, the presence of poorly crystalline alumina or silica in the products of γ-Al_2O_3 or kaolinite systems made phase quantification difficult. Mass balance for Si was accounted for by calculated masses of cristobalite and mullite, and there was no XRD evidence showing any Si-containing phase participated in Ni incorporation.

In terms of the reproducibility of these results, we replicated five experiments for A, B, D samples sintered at 1300 °C and the A1 sample sintered at 1250 °C by going through the mixing, pellet making, sintering, XRD scanning, and WPF procedure, independently. The observed half range between the maximum and the minimum estimated TR were ±1.5% (A), ±1.7% (B), ±2.7% (D), and ±1.4% (A1). The range of error, as shown by the error bar in Fig. 6, also reflected the heterogeneous nature and the less controlled quality of sintering the poorly mixed samples (like sample D). The *E*/*R* values of the WPF results shown in Fig. 6 range from 1.54 to 2.62. Most high *E*/*R* values came from refinements of those high TR samples. Fig. 7 shows the XRD patterns of 1480 °C and 3 h sintered ball-milled γ-Al_2O_3 + NiO slurry (A) sample (pattern a), and kaolinite + NiO

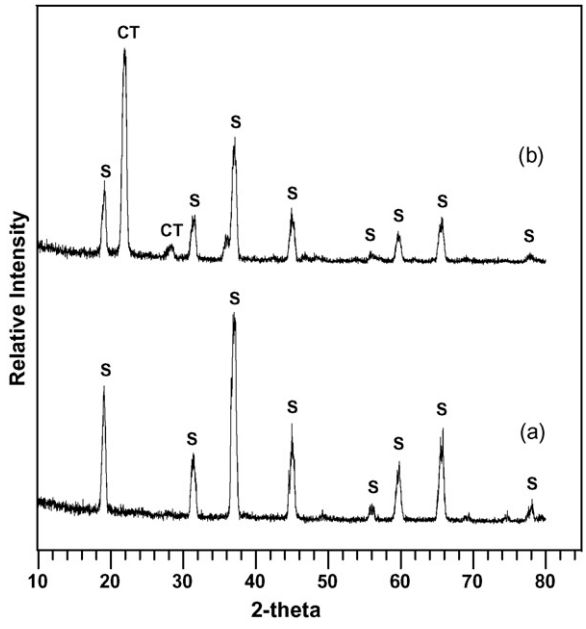

Fig. 7. XRD results of sintering (a) γ-Al_2O_3 + NiO slurry sample and (b) kaolinite + NiO slurry sample at 1480 °C for 3 h. "S" represents nickel aluminate spinel ($NiAl_2O_4$, ICDD PDF#78-0552); "CT" for cristobalite (SiO_2; ICDD PDF#76-0938).

slurry (A1) sample (pattern b). Both high TR patterns showed no noticeable NiO peaks (representing residual reactant), and the high-intensity $NiAl_2O_4$ peaks served as an example of the efficient incorporation of nickel into the spinel phase.

3.4. Leachability of sintered products

To evaluate the stabilization of nickel in sintered products, a nickel-leaching test was devised. The modified TCLP leaching experiment described earlier was used to evaluate the durability of NiO, $NiAl_2O_4$, and the product sintered from kaolinite + NiO. Both NiO and $NiAl_2O_4$ are known to be sparingly soluble, but in order to further differentiate the leachability among nickel phases, prolonged testing beyond that offered by the standard TCLP was required. The ball-milled γ-Al_2O_3 + NiO slurry (A) sample and kaolinite + NiO slurry (A1) sample sintered at 1480 °C for 48 h were selected for these leaching experiments. Prolonged high temperature sintering was used to further complete the NiO to $NiAl_2O_4$ spinel transforming reaction. The sintered samples were ground into powders and measured for BET surface area to yield values of $1.1 \pm 0.1\ m^2/g$ for $NiAl_2O_4$ and $0.83 \pm 0.14\ m^2/g$ for sintered kaolinite + NiO sample. Thirteen samplings were taken during the 0.75–25-day leaching period. Three independent replicates were made for the γ-Al_2O_3 + NiO and kaolinite + NiO samples, and two replicates were made for the NiO sample.

The pHs of the leachates are shown in Fig. 8. Within the first 3 days, there was a rapid increase in pH, but after 5 days the spinel product leachates stabilized with almost no increase in pH, while the NiO leachates exhibited a continuous increase in pH for the remainder of the experiment. The increase in pH arises from the dissolution of cations that exchange with protons in solution (effectively an acid/base reaction). This is accompanied by the destruction of crystals by the acidic leaching fluid. The continuous increases in leachate pH revealed NiO to be more vulnerable to proton-mediated dissolution. On the other hand, both $NiAl_2O_4$ spinel containing samples, the sintered γ-Al_2O_3 + NiO sample and kaolinite + NiO sample, showed stronger intrinsic resistance to the acidic attack.

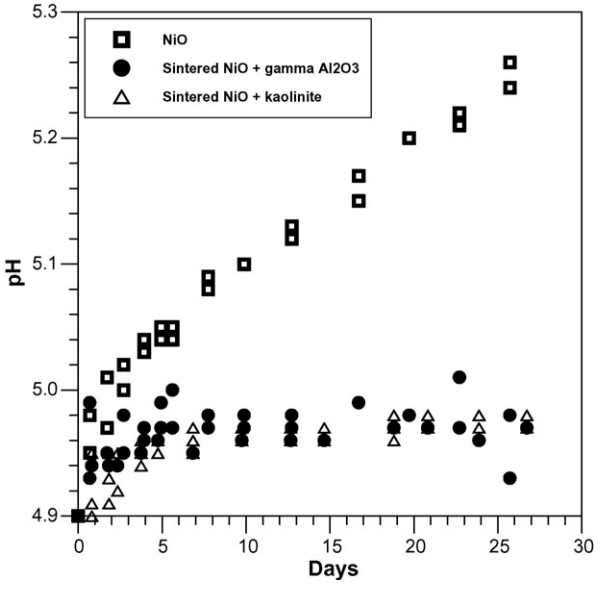

Fig. 8. pH values of sampled leachates of NiO, of 1480 °C/48 h sintered γ-Al_2O_3 + NiO sample ($NiAl_2O_4$), and of 1480 °C/48 h sintered kaolinite + NiO sample ($NiAl_2O_4$ + cristobalite). Each leaching vial was filled with 10 mL TCLP extraction fluid #1 (pH 4.9) and 0.5 g powder sample.

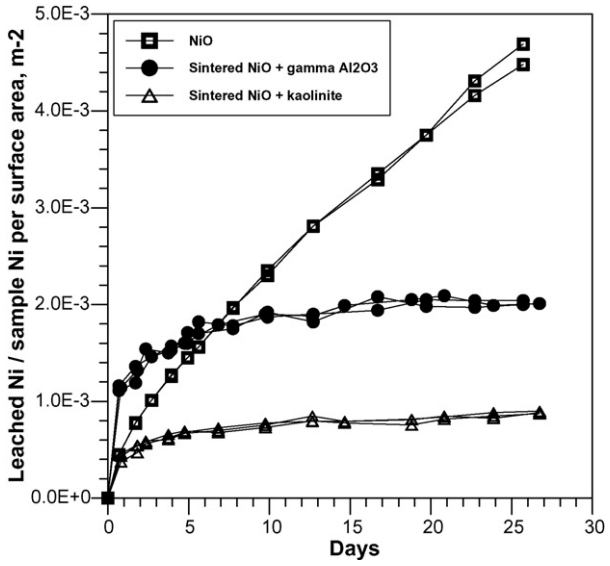

Fig. 9. Surface area and composition normalized ratios of leached to total nickel of NiO sample, of 1480 °C/48 h sintered γ-Al_2O_3 + NiO sample ($NiAl_2O_4$), and of 1480 °C/48 h sintered kaolinite + NiO sample ($NiAl_2O_4$ + cristobalite). The surface area of NiO powder was $3.6 \pm 0.5\ m^2/g$, of sintered γ-Al_2O_3 + NiO powder was $1.1 \pm 0.1\ m^2/g$ of sintered kaolinite + NiO powder was $0.83 \pm 0.14\ m^2/g$. Each leaching vial was filled with 10 mL TCLP extraction fluid #1 (pH 4.9) and 0.5 g powder sample.

Long-term leaching will be dominated by surface reactions, thus the leaching rate is likely to be proportional to surface area. In addition, since the same weight of sample was used for each leaching vial, the total nickel content in the sample, subject to different composition types, should also be normalized for comparison. Fig. 9 summarizes the nickel concentrations of the leachates normalized with respect to surface area and nickel content of leached solids. By this normalization, the nickel leachability of sintered γ-Al_2O_3 + NiO sample ($NiAl_2O_4$) seems to be similar to NiO in the first few days of leaching. Nevertheless, over longer time periods both spinel products were superior in nickel stabilization, shown by the much smaller increase in leachate nickel concentrations. Why the normalized leachability of sintered kaolinite + NiO sample was lower than leaching $NiAl_2O_4$ spinel (sintered γ-Al_2O_3 + NiO sample) alone is still uncertain. However, the effect might possibly be due to the better spinel crystallization and less weak grain boundaries promoted by the silica glass flux in sintering the NiO + kaolinite samples. It should be also noted that the standard TCLP (18 h) is incapable of distinguishing the relative leachabilities of these products, especially in predicting the long-term stability of ecomaterials.

Judging from the formation of $NiAl_2O_4$ spinel by sintering kaolinite + NiO, we can expect that Ni immobilization was taking place by two mechanisms: (i) a low temperature reaction between nickel oxide and a defect spinel and (ii) a high temper-

ature reaction between nickel oxide and mullite. The efficiency of incorporating Ni into $NiAl_2O_4$ spinel strongly depends on the sintering temperature, sintering time, and the mixing of raw materials. In most previous studies of sintering Ni waste and kaolinite-based clays,[18,19] the product phases should be NiO and $NiAl_2O_4$ spinel, except for other side reactions due to the complex composition of natural materials.[40] At most medium to low-grade tile or brick sintering temperatures (usually less than 1200 °C), nickel leachability of the products may be dominated by the relatively more leachable NiO phase. In this study, we suggest a preferred incorporation mechanism by forming $NiAl_2O_4$ at the higher but still attainable sintering temperatures to incorporate Ni-laden sludge into the kaolinite-based ceramic products.

4. Conclusions

Based on the reaction pathways and stabilization phases identified in this study, incorporation of nickel-laden waste sludge into kaolinite-based ceramic products showed great promise. The results of sintering kaolinite and nickel oxide mixtures between 990 and 1480 °C showed that $NiAl_2O_4$ spinel was the only new phase incorporating nickel. At lower temperature (990 °C), the $NiAl_2O_4$ formation mechanism was most likely the reaction between nickel oxide and the defect spinel generated from the kaolinite–mullite reaction series. The formation of $NiAl_2O_4$ by γ-Al_2O_3 and NiO mixture was also confirmed in this study at the same sintering condition. Besides sintering temperature and time, the mixing procedure for raw materials was also found to have great influence on the nickel incorporation efficiency. By performing four raw material mixing procedures, it was found the ball-milled slurry samples had the highest incorporation efficiency, which reached a transformation ratio (TR) greater than 90% with both γ-Al_2O_3 + NiO and kaolinite + NiO samples when sintered above 1250 °C for 3 h. In addition, silicon exists in cristobalite, amorphous silica, or mullite phases of the product, depending on sintering temperature and the composition ratio of raw materials, but no nickel was stabilized in any silicon phase with a sintering temperature below 1480 °C. In sintered kaolinite + NiO samples, aluminum existed in either $NiAl_2O_4$ or mullite; while in sintered γ-Al_2O_3 + NiO samples, it existed in either $NiAl_2O_4$ or corundum (α-Al_2O_3).

Results from prolonged TCLP leachability tests of NiO, $NiAl_2O_4$ (sintered from γ-Al_2O_3 + NiO samples), and sintered kaolinite + NiO samples indicate the $NiAl_2O_4$ containing samples showed stronger intrinsic resistance to acidic attack. In the 25-day leaching experiment by TCLP fluid #1 (pH 4.9), leachates of spinel products showed stabilized pH and nickel concentrations after few days, while the NiO leachates exhibited continuous increase in both pH and nickel concentration during the experiments. The leachability results revealed the superiority of $NiAl_2O_4$ over NiO in stabilizing nickel over long time periods. Nevertheless, results shown here also indicate that, at most medium to low-grade tile or brick sintering temperatures (usually less than 1200 °C), the nickel leachability of the products may be dominated by the relatively more leachable NiO phase. In this study, we demonstrated the feasibility of stabilizing nickel-laden sludge by kaolinite-base construction ceramics with the low intrinsic leachability of $NiAl_2O_4$ for better stabilization results.

Acknowledgements

The Alcoa Corporation is acknowledged for providing HiQ®-7223 alumina. Special thanks are due to Professor J.F. Stebbins for the use of equipment in pelletizing and sintering, to Mr. R.E. Jones for the assistance on XRD analysis, and to Dr. G. Li for the ICP Spectrometer metal measurements. We would also like to thank Professors T.J. White, S. Fendorf, M. Reinhard, and Dr. A.P. Robertson for fruitful discussions. Support from the Singapore Clean Water Programme and the Singapore Stanford Partnership is acknowledged.

References

1. Bolt, A., Tels, M. and van Gemert, W. J. T., Recovery of pure metal salts from mixed heavy metals hydroxides sludges. In *Recycling international: municipal waste, sewage sludge, hazardous and non-hazardous industrial waste, plastics and scrap types, food and beverage industry, packing, construction industry*, ed. K. J. Thome-Kozmiensky. EF-Verlag fur Energie-und Umwelttechnik, Berlin, Germany, 1984.
2. Andres, A., Ibanez, R., Ortiz, I. and Irabien, J. A., Experimental study of the waste binder anhydrite in the solidification/stabilization process of heavy metal sludges. *J. Hazard. Mater.*, 1998, **57**, 155–168.
3. Hirschhorn, J. and Oldenburg, K., *Prosperity without pollution: the prevention strategy for industry and consumers*. Van Nostrand Reinhold, New York, 1991.
4. Cheremisinoff, P. N. and Gigliello, K. A., *Leachate from hazardous waste sites*. TECHNOMIC Publishing, Lancaster, PA, 1983.
5. Bless, D., A review of electroplating nickel bath life extension, nickel recovery & copper recovery from nickel baths. *Plat. Surf. Finish.*, 2000, **87**(4), 72–78.
6. Roy, A., Eaton, H. C., Cartledge, F. K. and Tittlebaum, M. E., Solification/stabilization of a heavy metal sludge by a portland cement/fly ash binding mixture. *Hazard. Waste Hazard.*, 1991, **8**(1), 33–41.
7. Young, R. A., Toxicity summary for nickel and nickel compounds. http://risk.lsd.ornl.gov/tox/profiles/nickel_and_nickel_compounds_f_V1.shtml (accessed November 2005).
8. Ying, W. C., Bonk, R. R. and Tucker, M. E., Precipitation treatment of spent electroless nickel plating baths. *J. Hazard. Mater.*, 1988, **18**(1), 69–89.
9. Bolger, P. T. and Szlag, D. C., Investigation into the rejuvenation of spent electroless nickel baths by electrodialysis. *Environ. Sci. Technol.*, 2002, **36**(10), 2273–2278.
10. Anderson, R. W. and Neff, W. A., Electroless nickel bath recovery by cation-exchange and precipitation. *Plat. Surf. Finish.*, 1992, **79**(3), 18–26.
11. Horikawa, K. and Hirasawa, I., Removal and recovery of nickel ion from wastewater of electroless plating by reduction crystallization. *Korean J. Chem. Eng.*, 2000, **17**(6), 629–632.
12. National Renewable Energy Laboratory (NREL), Technologies for metal recovery save energy and reduce toxic metal wastes. http://es.epa.gov/techinfo/facts/technlgy.html (accessed July 2005).
13. Phifer, R. W. and McTigue, W. R., *Handbook of hazardous waste management for small quantity generators*. Lewis Publisher, Chelsea, MI, 1988.
14. Lewis, M. A., Fischer, D. F. and Smith, L. J., Salt-occluded zeolite as an immobilization matrix for chloride waste salt. *J. Am. Ceram. Soc.*, 1993, **76**(11), 2826–2832.
15. Sun, D., Wronkiewicz, D. J. and Simpson, L. J., A study of alteration phases on glass-bonded zeolite and sodalite using the vapor hydration test. In *Proceedings of the material research society symposium, vol. 556*, 1999, pp. 189–196.

16. Bernd, W. and Carl, F. S., Utilization of sewage sludge ash in the brick and tile industry. *Water Sci. Technol.*, 1997, **36**(11), 251–258.
17. Vieira, M. T., Catarino, L., Oliveira, M., Sousa, J., Torralba, J. M., Cambronero, L. E. G. *et al.*, Optimization of the sintering process of raw material wastes. *J. Mater. Process. Technol.*, 1999, **92/93**, 97–101.
18. Perez, J. A., Terradas, R., Manent, M. R., Seijas, M. and Martinez, S., Inertization of industrial wastes in ceramic materials. *Ind. Ceram.*, 1996, **16**(1), 7–10.
19. Douto, D. M. S., Silva, R. F., Castro, F. and Labrincha, J. A., Attempts of incorporation of metal plating sludges in ceramic products. *Ind. Ceram.*, 2001, **21**(3), 163–168.
20. Velde, B., *Introduction to clay minerals*. Chapman & Hall, London, UK, 1992.
21. Reed, J. S., *Principles of ceramics processing*. John Wiley & Sons, New York, 1995.
22. Brindley, G. W. and Nakahira, M., The kaolinite–mullite reaction series. I. A survey of outstanding problems. *J. Am. Ceram. Soc.*, 1959, **42**(7), 311–314.
23. Brindley, G. W. and Nakahira, M., The kaolinite–mullite reaction series. II. Metakaolin. *J. Am. Ceram. Soc.*, 1959, **42**(7), 314–318.
24. Schneider, H., Okada, K. and Pask, J. A., *Mullite and mullite ceramics*. John Wiley & Sons, New York, 1994.
25. Chen, C. Y. and Tuan, W. H., Evolution of mullite texture on firing tape-caste kaolin bodies. *J. Am. Ceram. Soc.*, 2002, **85**(5), 1121–1126.
26. Shih, K. and Leckie, J. O., Stabilizing simulated Ni-bearing sludge by aluminum-rich and iron-rich ceramic precursor. In *Proceedings of the joint clean water programme symposium*, 2005.
27. Diet, J. N., Moszkowicz, P. and Sorrentino, D., Behaviour of ordinary portland cement during the stabilization/solidification of synthetic heavy metal sludge: macroscopic and microscopic aspects. *Waste Manage.*, 1998, **18**, 17–24.
28. Phillips, B., Hutta, J. J. and Warsaw, I., Phase equilibria in the system $NiO–Al_2O_3–SiO_2$. *J. Am. Ceram. Soc.*, 1963, **46**(12), 579–583.
29. USEPA, Method 1311: Toxicity characteristic leaching procedure. http://www.epa.gov/epaoswer/hazwaste/test/pdfs/1311.pdf (accessed November 2005).
30. Zhou, R. S. and Snyder, R. L., Structures and transformation mechanisms of η, γ and θ transition aluminas. *Acta Crystallogr.*, 1991, **B47**, 617–630.
31. Wang, Y., Suryanarayana, C. and An, L., Phase transformation in nanometer-sized γ-alumina by mechanical milling. *J. Am. Ceram. Soc.*, 2005, **88**, 780–783.
32. Material Data, Inc., JADE 6.5.3 (computer software). Material Data, Inc., California, 2002.
33. Cesteros, Y., Salagre, P., Medina, F. and Sueiras, J. E., Synthesis and characterization of several $Ni/NiAl_2O_4$ catalysis active for the 1,2,4-trichlorobenzene hydrodechlorination. *Appl. Catal. B: Environ.*, 2000, **25**, 213–227.
34. Ross, J. R. H., Steel, M. C. F. and Zeini-Isfahani, A., Evidence for the participation of surface nickel aluminate sites in the stream reforming of methane over nickel/alumina catalysts. *J. Catal.*, 1978, **52**, 280–290.
35. Mocala, K. and Navrotsky, A., Structure and thermodynamic variation in nickel aluminate spinel. *J. Am. Ceram. Soc.*, 1989, **72**(5), 826–832.
36. Roelofsen, J. N., Peterson, R. C. and Raudsepp, M., Structure variation in nickel aluminate spinel ($NiAl_2O_4$). *Am. Mineral.*, 1992, **77**, 522–528.
37. Rahaman, M. N., *Ceramic processing and sintering*. Marcel Dekker, New York, 1995.
38. Lee, W. E. and Iqbal, Y., Influence of mixing on mullite formation in porcelain. *J. Eur. Ceram. Soc.*, 2001, **21**, 2583–2586.
39. Fansuri, H., Zhang, D. K., French, D., Elcombe, M. and Studer, A., An X-ray and neutron diffraction study of the structure of α-$Bi_2Mo_3O_{12}$ as a catalyst for partial oxidation of propylene to acrolein. In *Proceedings of the CHEMECA symposium, paper no. 234*, 2004.
40. Stegemann, J. A., Roy, A., Caldwell, R. J., Schilling, P. and Tittsworth, R., Understanding environmental leachability of electric arc furnace dust. *J. Environ. Eng.*, 2000, **126**, 112–120.